Chinese Chemical Letters 34 (2023) 107795

Contents lists available at ScienceDirect

Chinese Chemical Letters

journal homepage: www.elsevier.com/locate/cclet

Near infrared light-induced dynamic modulation of enzymatic activity through polyphenol-functionalized liquid metal nanodroplets

Chaojun Zhang[a], Yang Tang[a], Qin Wang[a,b], Yunxiang He[a,c], Xiaoling Wang[a,c,*], Sebastian Beyer[d], Junling Guo[a,c,e,f,*]

[a] BMI Center for Biomass Materials and Nanointerfaces, College of Biomass Science and Engineering, Sichuan University, Chengdu 610065, China
[b] School of Pharmacy, Southwest Minzu University, Chengdu 610225, China
[c] National Engineering Research Center of Clean Technology in Leather Industry, Sichuan University, Chengdu 610065, China
[d] Department of Biomedical Engineering, Chinese University of Hong Kong, Hong Kong 999077, China
[e] State Key Laboratory of Polymer Materials Engineering, Sichuan University, Chengdu 610065, China
[f] Bioproducts Institute, Department of Chemical and Biological Engineering, University of British Columbia, Vancouver, BC V6T 1Z4, Canada

ARTICLE INFO

Article history:
Received 21 July 2022
Revised 18 August 2022
Accepted 1 September 2022
Available online 17 October 2022

Keywords:
Enzymatic activity
Photo-modulation
Near infrared light
Liquid metal nanodroplets
Metal-phenolic nanocoating

ABSTRACT

Dynamic manipulation of enzymatic activity is a challenging task for applications in chemical and pharmaceutical industries due to the difficult modification and variable conformation of various enzymes. Here, we report a new strategy for reversible dynamic modulation of enzymatic activity by near-infrared light-induced photothermal conversion based on polyphenol-functionalized liquid metal nanodroplets (LM). The metal-phenolic nanocoating not only provides colloidal stability of LM nanodroplets but also generates nanointerfaces for the assembly of various enzymes on the LM nanodroplets. Upon near infrared (NIR) irradiation, the localized microenvironmental heating through photothermal effect of the LM nanodroplets allows tailoring the enzymatic activity without affecting the bulk temperature. A library of functional enzymes, including proteinase K, glucoamylase, glucose oxidase, and Bst DNA polymerase, is integrated to perform a reversible control and enhanced activities even after five times of cycles, demonstrating great potential in bacterial fermentation, bacteriostasis, and target gene amplification.

The precise control of enzymatic activities remotely and spatiotemporally by using an external stimulus is highly desirable in a wide range of enzymatic-based chemical and biological applications [1–6]. The photo-regulation of enzymatic activity evolves as promising alternatives for enzyme modulation during the industrial manufacturing and biological processes owing to its unique advantages of noninvasiveness and spatiotemporal specificity [7–12]. However, for the lack of natural photocatalytic ability of enzyme that can harness light-energy for industrial manufacturing, a hybrid system has been engineered that integrates the catalytic capabilities of enzymes with external photochemical and light-responsive molecules, especially for the near infrared (NIR) light, which often needs to balance the competing interests of improving enzymatic activity and maintaining well-defined three-dimensional protein structures [13–15]. Apart from these organic molecules, metal nanoparticles as typical inorganic materials, because of inherently efficient photothermal effect for NIR light, have also been broadly exploited for repeated manipulation of enzymatic activity, which usually immobilizes enzymes on the surfaces of metal nanoparticles, allowing for local heating through this metal nanoparticle-associated photothermal effect upon NIR irradiation [16–19]. Inevitably, to immobilize the biocatalyst on these inorganic "rigid" supporting materials, the introduction of covalent bonds on the surface-functionalized inorganic nanoparticles is necessary, which however, mostly causes the deformation of enzymes and leads to the dramatic decrease of enzymatic activities.

In contrast to these "rigid" solid metal nanomaterials, the droplets of liquid metal (LM) show outstanding photochemical and photothermal conversion properties. Its applications in diverse functional systems ranging from soft electronics to photothermal therapy (PTT) of tumor have been expanded [20,21]. This is mainly attributed to the collective electron oscillations on its surface that can be utilized to efficiently convert optical energy to thermal energy under various wavelength of light and easily adjustable size [21]. While its large surface tension (624 mN/m), oxide shells, and poor compatibility with most other materials prevent uniform dispersion of LM droplets and hybridization into composites, except the application of external interventions (*e.g.*, shear

* Corresponding authors.
E-mail addresses: xlwang@scu.edu.cn (X. Wang), junling.guo@scu.edu.cn, junling.guo@ubc.ca (J. Guo).

https://doi.org/10.1016/j.cclet.2022.107795
1001-8417/

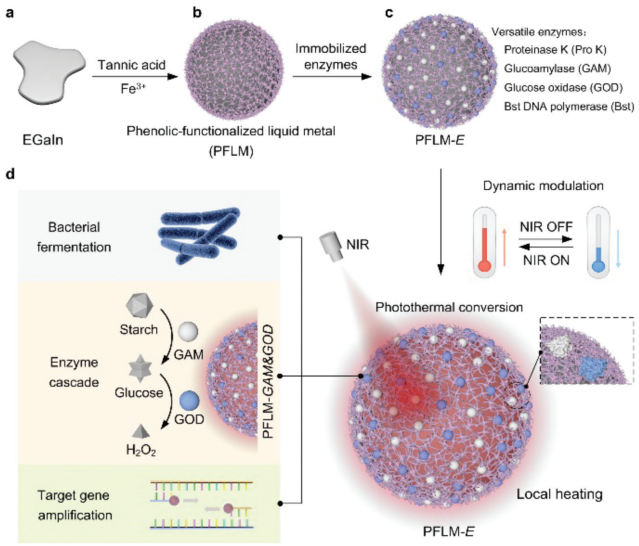

Fig. 1. Preparation of PFLM-*E* and schematic diagram of PFLM-*E* activity modulation by NIR light. (a-c) Illustration depicts the synthesis of PFLM-*E*. (d) The accelerated bacterial fermentation, enzyme cascade reaction, and target gene amplification by manipulating activity of PFLM-*E* using NIR light.

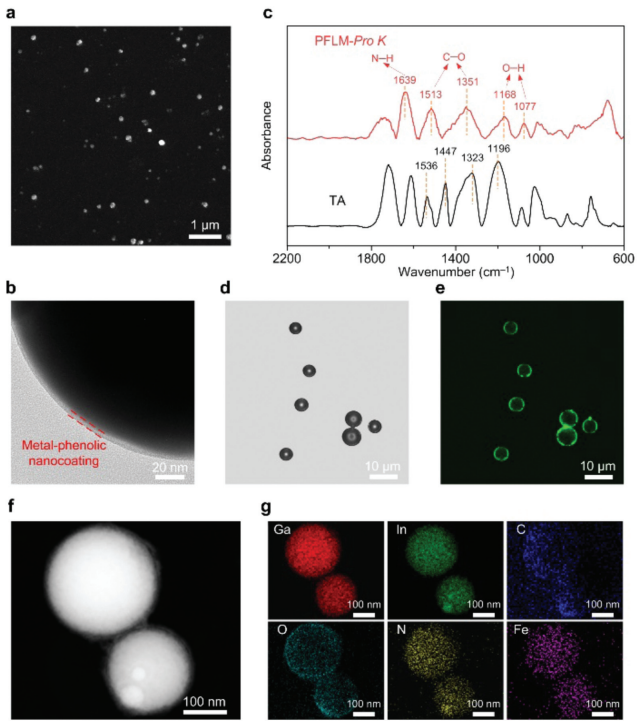

Fig. 2. Characterization of PFLM-*E*. (a) FESEM micrographs showing the spherical shape of PFLM. (b) TEM image showing the PFLM nanodroplets and self-assembled metal-phenolic nanocoating on the surface of PFLM. (c) FTIR spectra of TA and PFLM-*Pro K*. (d, e) CLSM images of PFLM-*Pro K*. (f, g) HAADF-STEM and EDX mapping images of PFLM-*Pro K*.

and laser) [22–24]. Recently, the nature of stabilizing molecules for LM dispersions provides functional coatings to change the surface chemistry of LM droplets and generate stable colloidal LM nanodroplets [25–28]. For accessing new surface functionalization, polyphenols, sustainable biomass abundant in nature, are ideal substrate-independent candidates for their rich galloyl or catechol groups, that display non-substrate-specific by high binding affinity (diverse covalent and/or noncovalent interactions) [29–32]. Meanwhile, the traditional tanning chemistry of leather indicates that these galloyl or catechol groups of polyphenols can facilitate noninterfering interactions (such as hydrogen bond) with proteins without irreversible destructions in the conformation of protein molecules [33].

Here, we reported a polyphenol-functionalized LM nanodroplet (PFLM) integrated with a range of functional enzymes (PFLM-*E*) that enable the dynamic manipulation of their catalytic activities by NIR light. The galloyl or catechol groups of polyphenols provide stabilization on the LM into nanodroplets by the coordination with metal ions of LM surface. Moreover, different enzymes can be integrated on the surfaces of PFLM nanodroplets through the noninterfering interactions of polyphenols. Upon NIR irradiation, local heating through photothermal effect of the LM nanodroplets from PFLM-*E* allows a precise control of the enzymatic activities without affecting the bulk temperature. The enzymatic activity was significantly enhanced to 4.4-fold during NIR irradiation, and further tunable by varying irradiation times and laser power densities. Four types of enzymes including proteinase K (Pro K), glucoamylase (GAM), glucose oxidase (GOD), and Bst DNA polymerase (Bst) were successfully engineered with NIR-tunable enzymatic activity based on PFLM nanosystems, and further demonstrated for their applications in bacterial fermentation, bacteriostasis, and target gene amplification.

The preparation of PFLM-*E* using a top-down approach is schematically presented in Fig. 1. Because of the diverse chelation ability of phenolic compounds, tannic acid (TA), a ubiquitous natural polyphenol, was coordinated to intrinsic Ga^{3+} ions and external Fe^{3+} ions during the disintegration of large eutectic LM (eutectic gallium-indium, EGaIn) droplets into stable nanodroplets by ultrasonic stimulation (at 500 W for 30 min) [34–36]. Thus, a robust and dense metal-phenolic nanocoating can be formed on the surfaces of LM nanodroplets to stabilize the colloidal LM nanodroplets and also prevent accumulation of LM nanodroplets induced by their high surface tension (Figs. 1a and b). Furthermore, due to the noninterfering interactions of catechol or galloyl groups for proteins, various enzymes (including Pro K, GAM, GOD and Bst) were flexibly immobilized on the metal-phenolic nanocoatings of PFLM, named as PFLM-*E* (*E* represents different enzymes, Fig. 1c and Table S1 in Supporting information). The PFLM-*E* allows local heating through photothermal effect of the LM upon NIR irradiation that enables manipulation of catalytic activity of the PFLM-*E* by NIR light and can be applied to bacterial fermentation, enzyme cascade reaction, and target gene amplification (Fig. 1d).

Field emission scanning electronic microscopy (FESEM) image revealed that PFLM nanodroplets were highly monodispersed, and their average diameter sizes were 100–200 nm (Fig. 2a), which was consistent with findings of dynamic light scattering (DLS) analyses (170 ± 50 nm, Fig. S1 in Supporting information). Transmission electronic microscopy (TEM) performed on the PFLM nanodroplets also confirmed the spherical shapes of PFLM, and the presence of metal-phenolic nanocoatings on the surfaces of PFLM nanodroplets, with an observed thickness around 6 nm (Fig. 2b and Fig. S2 in Supporting information). The ultraviolet-visible (UV–vis) absorption spectra of the supernatant obtained after disassembly of the metal-phenolic nanocoatings of PFLM nanodroplets indicated the presence of polyphenol-based functionalization on LM nanodroplets (Fig. S3 in Supporting information). X-ray photoelectron spectroscopy (XPS) analysis further revealed the interaction between TA, LM, and Fe^{3+} (Figs. S4 and S5 in Supporting information). Compared with the high-resolution XPS O 1s spectra of TA, the peak (C–O) of PFLM shifted to higher binding energy, from 533.2 eV to 533.4 eV, as the TA interacted with metal ions (Ga^{3+} and Fe^{3+}). From the core-level XPS spectra of Ga 3d of LM, the peak centered at binding energy of 19.8 eV was assigned to Ga^{3+},

and the peak in Ga^{3+} 3d spectra of the PFLM nanodroplets was shifted to higher energy (20.6 eV). These differences demonstrated that the coordination between TA and metal ions (Ga^{3+} and Fe^{3+}) had occurred on the surfaces of PFLM nanodroplets. In addition, the C–O (533.2 eV) peak in O 1s spectra of PFLM-*Pro K* also moved to higher energy than that of PFLM, and a new organonitrogen peak appeared at 399.2 eV in the N 1s spectra of PFLM-*Pro K*, indicating that the Pro K had been successfully immobilized on the surfaces of PFLM-*Pro K* nanodroplets.

Fourier transform infrared (FTIR) spectroscopic analyses of TA and PFLM-*Pro K* nanodroplets showed in Fig. 2c. The vibrational peaks characteristic of TA, phenolic C–O stretching bands at 1536 and 1447 cm^{-1}, and phenolic O–H bending vibrations at 1323 and 1196 cm^{-1}, were shifted to 1513, 1351 cm^{-1}, and 1168, 1077 cm^{-1}, respectively, in the PFLM-*Pro K* nanodroplets. This further suggested the coordination of Ga^{3+} and Fe^{3+} on the surfaces of PFLM nanodroplets with the catechol/galloyl groups of TA [37]. The strong vibration peak at 1639 cm^{-1} might be ascribed to N–H stretching vibration of Pro K in PFLM-*Pro K*. Raman spectroscopy analysis of the PFLM-*Pro K* also suggested the coordination of TA on the PFLM nanodroplet surface (Fig. S6 in Supporting information). Meanwhile, the successful immobilization of Pro K was confirmed by the uniform distribution of fluorescein isothiocyanate-labeled Pro K fluorescence observed in confocal laser scanning microscope (CLSM) images (Figs. 2d and e). High-angle annular dark-field scanning TEM (HAADF-STEM) image (Fig. 2f) and energy dispersive X-ray spectroscopy (EDX) mapping (Fig. 2g) of the PFLM-*Pro K* nanodroplets demonstrated the element composition of PFLM-*Pro K* as the evident from the spatially concentrated signals of uniformly distributed C, O, N and Fe appearing from interfacial organic metal-phenolic nanocoatings. The C, O and N elements coincided well with Ga and In elements from LM, which proved the immobilization of Pro K on the surfaces of PFLM nanodroplets. Additionally, after immobilization, GAM, as a typical enzyme with a large molecular diameter (10 nm), was also successfully immobilized on the PFLM nanodroplet surface (Fig. S7 in Supporting information).

Pro K is an enzyme that widely used in food biotechnology and molecular biology because of its broad substrate specificity for hydrolysis of esters as well as its ability to cleave the peptide bond proximate to the carboxyl group of aliphatic and aromatic amino acids. Normally, its activity is enhanced by increasing temperature of the whole catalytic system to improve the hydrolysis, which is high energy-consumption. When the Pro K was immobilized on the PFLM nanodroplet surface, the enzymatic activity of Pro K in PFLM-*Pro K* could be changed by exposure to NIR light. PFLM nanodroplets played a role in tailoring the enzymatic activity of Pro K for hydrolyzing sodium caseinate into various amino acids (tyrosine, tryptophan, and phenylalanine, *etc*.) due to the photothermal response property of PFLM nanodroplets (Fig. 3a).

The superposition circular dichroism (CD) spectra of Pro K and TA-Pro K revealed that the secondary structure of Pro K barely changes before and after the integration with PFLM, supporting the immobilization of Pro K was based on noninterfering interactions (Fig. 3b). A range of other functional enzymes (GAM, GOD, and Bst of PFLM-*GAM*, PFLM-*GOD* and PFLM-*Bst*) could also maintain their catalytic activities after the integration with PFLM (Fig. S8 in Supporting information). The enzymatic activity of TA-Pro K for hydrolyzing sodium caseinate into amino acids was detected by high performance liquid chromatography (Fig. S9 in Supporting information). Compared with that of Pro K, the enzymatic activity of TA-Pro K could be retained by over 90% with the increased TA concentration from 1×10^{-5} mol/L to 10×10^{-5} mol/L. These results indicated that the noninterfering interactions between TA and enzymes are unlikely induce irreversible destructions.

The catalytic activities of PFLM-*Pro K* incubated at NIR irradiation of different power densities for 10 min were investigated in Fig. 3c. With the increase of laser power densities of NIR, the catalytic activity of PFLM-*Pro K* was significantly enhanced, up to 3.0-fold at the power density of 4.0 W/cm^2. Moreover, when the irradiation time was increased, the catalytic activity of PFLM-*Pro K* was also significantly enhanced (Fig. 3d). After irradiating 15 min at the power density of 3.0 W/cm^2, the catalytic activity of PFLM-*Pro K* could be increased 4.4 times as much as the initial state. Interestingly, during the enhancement of the PFLM-*Pro K* catalytic activity, the temperature of the whole reaction system just changed slightly (from 25.5 °C to 29.9 °C) under NIR irradiation, that was, the increased activity of PFLM-Pro K was due to the environmental nanoscale heating caused by the absorption of LM nanodroplets (2 mg/mL) under NIR irradiation (Fig. S10 in Supporting information).

The switch-on catalytic activity of PFLM-*Pro K* was further examed. The results showed that the catalytic activity of PFLM-*Pro K* was reversibly regulated and increased rapidly when irradiated by NIR light, but decreased to a normal level without the NIR irradiation (Fig. 3e). In addition, we could easily re-collect PFLM-*Pro K* since LM is denser than water, and the recovering PFLM-*Pro K* could be employed in the next cycled catalytic reaction. After five cycled catalytic reactions, the recovering catalytic activity of PFLM-*Pro K* still retained 1.5 times over that of the initial Pro K (Fig. 3f). Similarly, the catalytic activity of PFLM-*GAM* was also increased with the increased NIR power densities from 1.0 W/cm^2 to 4.0 W/cm^2, and the corresponding catalytic activity was up to 1.7-fold at the power density of 4.0 W/cm^2 (Fig. S11 in Supporting information). Importantly, the temperature of the whole reaction system only changed slightly from 26.2 °C to 31.7 °C. Additionally, the catalytic activity of PFLM-*GAM* could be increased 1.9 times as much as the initial GAM with the enhancement of irradiation time to 15 min at the power density of 3.0 W/cm^2 (Fig. S12 in Supporting information). And the temperature of the PFLM-*GAM* reaction system also changed slightly (from 26.0 °C to 29.8 °C). The catalytic activity of PFLM-*GAM* could be also tuned reversibly and responded rapidly to NIR irradiation (Fig. S13 in Supporting information). After five cycled catalytic reactions, the recovering catalytic activity of PFLM-*GAM* still retained 1.5 times that of the initial state (Fig. S14 in Supporting information).

For industrial fermentation (such as lactic acid fermentation), highly efficient protease hydrolysis system is a common solution to promote the rapid growth of beneficial bacteria (lactic acid bacteria) to shorten the processing time of fermented products and improve the flavor and nutrients of the food [38,39]. While, because nitrogen sources from large molecular proteins in the fermentation system are difficult to use directly by beneficial bacteria. These large-molecular proteins (such as sodium caseinate) in this system are usually needed to degrade into short peptides and amino acids for offering nitrogen sources under the catalytic action of Pro K, thus supporting the rapid growth of lactic acid bacteria and shortening the fermentation time. To increase Pro K activity, the system of fermentation is often exposed to high temperature, but it causes damage to the nutrition and affects the food taste. To avoid this challenge, we irradiated PFLM-*Pro K* with NIR light to increase the localized microenvironmental temperature of Pro K by taking advantage of the photothermal conversion ability of PFLM. The localized microenvironmental heating promotes the hydrolysis of sodium caseinate through Pro K and further improves reproduction and metabolism of lactic acid bacteria, thus achieving the purpose of accelerating the fermentation of food without destroying nutrients and flavors (Fig. 3g). Under the NIR light irradiation, the large-molecular proteins (sodium caseinate) could be hydrolyzed into diverse amino acids for offering the nitrogen sources without significant temperature change of the whole fermentation system.

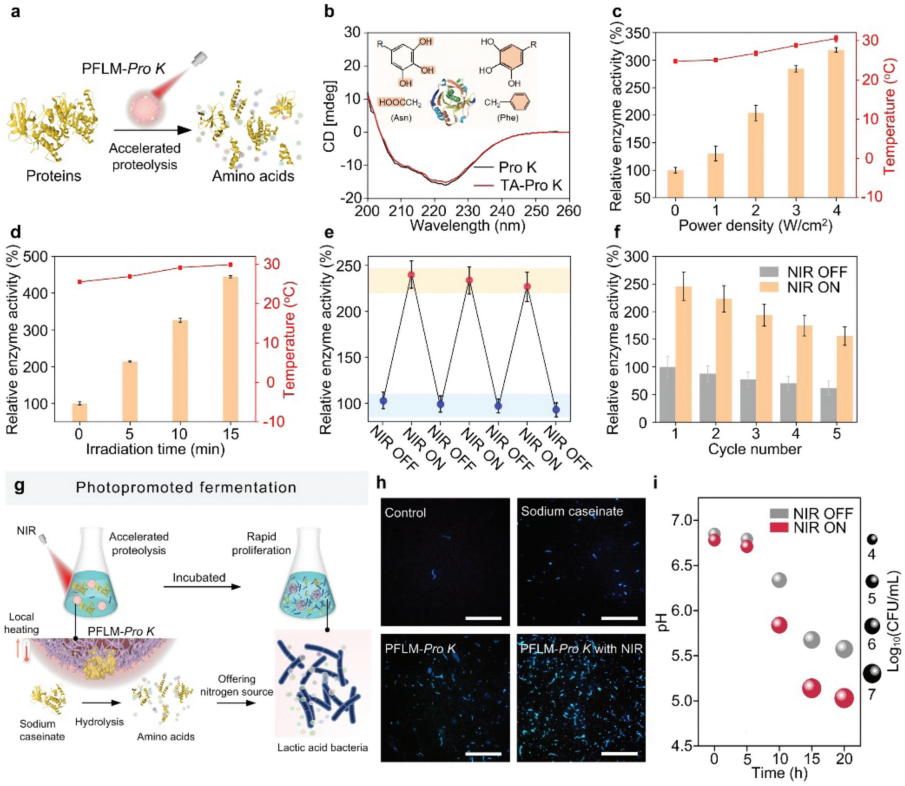

Fig. 3. NIR light modulating the catalytic activity of PFLM-*Pro K* and accelerating industrial fermentation. (a) Illustration of the accelerated proteolysis by PFLM-*Pro K* with NIR irradiation. (b) CD spectra of Pro K and TA-Pro K. Inset: Schematic diagram of the possible interactions between the functional groups of polyphenols and proteins. (c) Catalytic activities of PFLM-*Pro K* upon pulse NIR irradiation at different power densities for 10 min. (d) Catalytic activities of PFLM-*Pro K* by exposure to pulse NIR laser for different times. (e) The reversibility of modulating catalytic activity of PFLM-*Pro K* was evaluated by exposing to cycled pulse NIR irradiations (3.0 W/cm^2, 10 min for each cycle). (f) The cycled catalytic activity of PFLM-*Pro K* with irradiation at 3.0 W/cm^2 for 10 min. (g) Schematic showing improved hydrolysis of sodium caseinate by PFLM-*Pro K* with NIR irradiation to promote lactic acid bacteria reproduction and fermentation. (h) Fluorescence microscopy images of lactic acid bacteria incubated for 20 h with/without sodium caseinate and promoting proteolysis by PFLM-*Pro K* with/without NIR irradiation on sodium caseinate. Scale bar = 5 μm. (i) The pH value and number of lactic acid bacteria during the incubation after promoting proteolysis by PFLM-*Pro K* with/without NIR irradiation on sodium caseinate.

Under NIR light irradiation, PFLM-*Pro K* showed a higher catalytic activity and produced more free amino acids as nitrogen sources for lactic acid bacteria (Figs. S15 and S16 in Supporting information), which increases the number of lactic acid bacteria (Figs. S17 and S18 in Supporting information), supported by the higher intensity of cytoplasmic fluorescence (Fig. 3h and Fig. S19 in Supporting information) than that of hydrolysis system of sodium caseinate by PFLM-*Pro K* without NIR irradiation. Additionally, because the proliferation of lactic acid bacteria produced more metabolites (lactic acid) in the hydrolysis system of sodium caseinate by PFLM-*Pro K* with NIR light irradiation, the pH value decreased rapidly (from 6.8 to 5.0), thus delivering into a rapid fermentation (Fig. 3i).

Multienzyme cascade that mediates multistep chemical reactions in one-pot systems can avoid the isolation/purification of intermediates and shift the reaction equilibrium to the product side, which is a most important technology to succeed in industrial process development [40,41]. PFLM can simultaneously assemble multiple enzymes to achieve the effect of cascade catalysis due to the non-specific multiple noninterfering interactions between TA and various enzymes.

In our multienzyme cascade model, GAM digests starch into glucose, and GOD can further catalyze the oxidation of glucose into gluconolactone and H_2O_2, inducing oxidative stress damage of bacteria. We prepared a dual-enzymatic PFLM-*GAM&GOD*, and under the NIR irradiation, the final decomposition products present antibacterial activity after diffusion in solidified agar plate as GAM and GOD cascade catalyzed starch into H_2O_2 (Fig. 4a). Upon NIR irradiation, GAM and GOD of PFLM-*GAM&GOD* showed significantly enhanced enzymatic activity, and more H_2O_2 was produced to enlarge the diameter of antibacterial zone (22 mm) that larger than that of PFLM-*GAM&GOD* (15 mm) without NIR irradiation (Fig. 4b), indicating the stronger antibacterial effect and improvement of cascade catalysis of PFLM-*GAM&GOD* with NIR irradiation. In addition, the systems of PFLM-*GAM* and PFLM-*GOD* showed no antibacterial activity due to the inability to hydrolyze starch to H_2O_2 when GAM and GOD were present alone in PFLM-*GAM* and PFLM-*GOD*, respectively. Thus, the corresponding diameters of antibacterial zones were kept at 6 mm without any enlargements. Besides, the photothermal effect of PFLM had no bacteriostasis as the diameters of antibacterial zone were still kept at 6 mm (Fig. S20 in Supporting information). These results suggested that the antibacterial activity of the catalytic system of PFLM-*GAM&GOD* with NIR irradiation mainly arises from the cascade hydrolysis products (H_2O_2) induced by the multiple enzymatic reactions (GAM and GOD). Moreover, the antibacterial activity of PFLM-*GAM&GOD* could be enhanced by the NIR irradiation, because the activities of GAM and GOD of PFLM-*GAM&GOD* were improved simultaneously for the increased localized microenvironmental temperature of GAM and GOD by taking advantage of the photothermal conversion ability of PFLM, thus accelerating the multienzyme cascade.

DNA polymerase plays a pivotal role in gene amplification, which is of great significance for point-of-care (POC) testing in prevention and treatment of disease [42]. However, gene amplification often requires sophisticated laboratory equipment, and in-

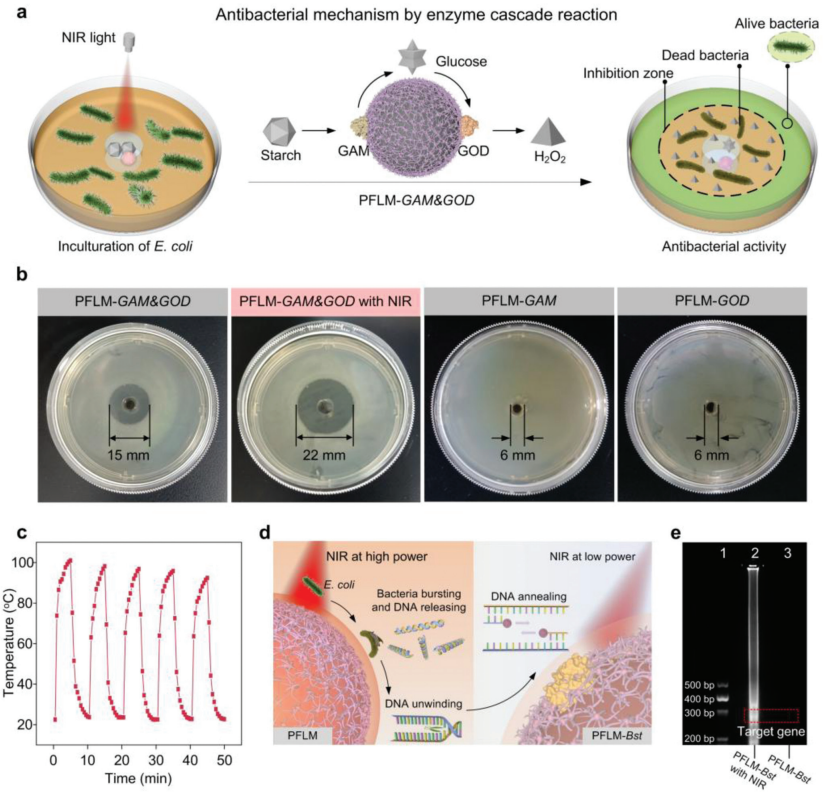

Fig. 4. Regulation of enzyme cascade antibacterial activity and remote gene amplification by NIR light. (a) Schematic illustrated NIR irradiation enhanced production of H_2O_2 by PFLM-*GAM&GOD* for antibacteria. (b) The antibacterial activity of PFLM-*GAM&GOD* upon NIR irradiation (0.5 W/cm^2 for 1 h) by determining inhibition zone diameter in the presence of soluble starch. (c) Photothermal effects of PFLM nanodroplets (at 3.8 W/cm^2, 10 min for each cycle). (d) Schematic of remote LAMP based on PFLM-*Bst* photothermal conversion. (e) Electrophoretic analysis of target gene amplification under PFLM-*Bst* with/without NIR irradiation.

creases the energy and time consumed in heat transfer due to the characteristics of contact heating [43]. PFLM is a highly efficient converter of energy from light to located microenvironmental heat, and its noncontact heating and fast thermocycling rate could minimize the energy and time consumption in the heat transfer process. The photothermal effect of LM becomes better as the droplet size decreases gradually (Fig. S21 in Supporting information). Under NIR light irradiation (at 3.8 W/cm^2), the dispersion temperature of 170 nm PFLM nanodroplets (40 mg/mL) increased to 95 °C within 3 min, and five on/off cycles of NIR irradiation test confirmed the superior photostability of PFLM (Fig. 4c).

Thus, we regulated the temperature change of the PFLM-*Bst* nanodroplets by adjusting the power density of NIR light to achieve ultra-fast thermal transfer and enhance Bst enzymatic activity for microscale gene amplification (Table S2 in Supporting information) by loop-mediated isothermal amplification (LAMP). When the PFLM nanodroplets were added to the *Escherichia coli* O157:H7 (*E. coli* O157:H7) dispersion, the photothermal effect of PFLM nanodroplets made their bulk temperature higher than 95 °C with NIR irradiation at high power density (3.8 W/cm^2) for 10 min (Fig. S22 in Supporting information), which could rupture *E. coli* O157:H7 to release DNA and unwind DNA into single-stranded DNA (Fig. 4d). Then, after adding the PFLM-*Bst* nanodroplets and changing the power density of NIR light to 2.0 W/cm^2 for 1 h, single-stranded DNA was annealed into double-stranded DNA under the improved catalysis of PFLM-*Bst* with reduced bulk temperature (60 °C), thus achieving a simple and rapid amplification of the target gene. The correct band location (299 bp) of the target gene from *E. coli* O157:H7 was obtained by gel electrophoresis [44], while no bands were found on agarose gel electrophoresis under the same condition without NIR irradiation (Fig. 4e). These results proved that the engineered PFLM-*Bst* successfully amplified the target gene through the precise control of PFLM-*Bst* activity with NIR irradiation.

In summary, we reported phenolic-functionalized liquid metal nanodroplets assembled with various enzymes for dynamic control of enzymatic activity by NIR irradiation. The polyphenol-based nanocoating provides stabilization of LM, obtaining colloidally-stable LM nanodroplets (PFLM). A variety of a single or multiple enzymes can be integrated on the surface of PFLM to generate biohybrid PFLM-*E* nanosystems, in which NIR irradiation can be converted to localized microenvironmental heating to achieve a NIR-induced dynamic modulation of enzymatic activities. Moreover, PFLM-*E* showed reusable and reversible activities in subsequent five-cycle experiments. We designed three types of PFLM-*E* nanosystems by integrating a library of functional enzymes, including proteinase K, glucoamylase-glucose oxidase cascade, and Bst DNA polymerase, and demonstrated their potential applications in industrial fermentation, bacteriostasis, and target gene amplification. Our study provides a facile and efficient strategy to realize the dynamic control of enzymatic activity by NIR irradiation, which has potential applications in more complex biological and industrial applications.

Declaration of competing interest

The authors declare that they have no known competing financial interests or personal relationships that could have appeared to influence the work reported in this paper.

Acknowledgments

We would like to thank X. He at the College of Biomass Science and Engineering of Sichuan University for characterization as-

sistance. We also appreciate H. Wang from the Analytical & Testing Center of Sichuan University for the help with SEM characterizations. We acknowledge financial support from the National Talents Program, National Natural Science Foundation of China (Nos. 22178233, 22108181), Talents Program of Sichuan Province, Double First-Class University Plan of Sichuan University, State Key Laboratory of Polymer Materials Engineering (No. sklpme 2020−03−01), and the Sichuan Province Postdoctoral Special Funding.

References

[1] R.A. Sheldon, J.M. Woodley, Chem. Rev. 118 (2018) 801–838.
[2] S. Zhang, S. Liu, Y. Sun, et al., Chem. Soc. Rev. 50 (2021) 13449–13466.
[3] P. Intasian, K. Prakinee, A. Phintha, et al., Chem. Rev. 121 (2021) 10367–10451.
[4] E.M. Zhao, Y. Zhang, J. Mehl, et al., Nature 555 (2018) 683–687.
[5] K.G. Kumaraswamy, A. Krishnan, G. Ananyev, et al., Energ. Environ. Sci. 12 (2019) 1035–1045.
[6] M. Wensien, F.R. von Pappenheim, L.M. Funk, et al., Nature 593 (2021) 460–464.
[7] X.X. Zhou, L.Z. Fan, P. Li, et al., Science 355 (2017) 836–842.
[8] A.H.G. David, R. Casares, J.M. Cuerva, et al., J. Am. Chem. Soc. 141 (2019) 18064–18074.
[9] J.A. Frank, D.A. Yushchenko, D.J. Hodson, et al., Nat. Chem. Biol. 12 (2016) 755–762.
[10] T. Tian, Y. Song, J. Wang, et al., J. Am. Chem. Soc. 138 (2016) 955–961.
[11] K. Chen, F.H. Arnold, Nat. Catal. 3 (2020) 203–213.
[12] Y. Zhou, C. Zhou, Nat. Chem. 13 (2021) 299–301.
[13] C. Xu, W. Bing, F. Wang, et al., ACS Nano 11 (2017) 7770–7780.
[14] A.V. Leopold, K.G. Chernov, A.A. Shemetov, et al., Nat. Commun. 10 (2019) 1129.
[15] S. Chen, A.Z. Weitemier, X. Zeng, et al., Science 359 (2018) 679–684.
[16] C. Wang, Q. Zhang, X. Wang, et al., Angew. Chem. Int. Ed. 56 (2017) 6767–6772.
[17] S. Zhang, C. Wang, H. Chang, et al., Sci. Adv. 5 (2019) eaaw4252.
[18] H.R. de Barros, I. García, C. Kuttner, et al., ACS Catal. 11 (2020) 414–423.
[19] S.A. Thompson, S. Paterson, M.M. Azab, et al., Small 13 (2017) 1603195.
[20] E.J. Markvicka, M.D. Bartlett, X. Huang, et al., Nat. Mater. 17 (2018) 618–624.
[21] S.A. Chechetka, Y. Yu, X. Zhen, et al., Nat. Commun. 8 (2017) 15432.
[22] Y. Liu, W. Zhang, H. Wang, Mater. Horiz. 8 (2021) 56–77.
[23] C.J. Thrasher, Z.J. Farrell, N.J. Morris, et al., Adv. Mater. 31 (2019) e1903864.
[24] X. Li, M. Li, L. Zong, et al., Adv. Funct. Mater. 28 (2018) 1804197.
[25] X. Li, M. Li, J. Xu, et al., Nat. Commun. 10 (2019) 3514.
[26] Y. Lu, Q. Hu, Y. Lin, et al., Nat. Commun. 6 (2015) 10066.
[27] J. Yan, M.H. Malakooti, Z. Lu, et al., Nat. Nanotechnol. 14 (2019) 684–690.
[28] F. Centurion, M.G. Saborio, F.M. Allioux, et al., Chem. Commun. 55 (2019) 11291–11294.
[29] J. Chen, S. Pan, J. Zhou, et al., Adv. Mater. (2021) e2108624.
[30] M. Shin, H.A. Lee, M. Lee, et al., Nat. Biomed. Eng. 2 (2018) 304–317.
[31] D.J.A. Jenkins, C.W.C. Kendall, J.L. Sievenpiper, J. Am. Coll. Cardiol. 78 (2021) 679–682.
[32] J. Guo, B.L. Tardy, A.J. Christofferson, et al., Nat. Nanotechnol. 11 (2016) 1105–1111.
[33] Y. Han, Z. Lin, J. Zhou, et al., Angew. Chem. Int. Ed. 59 (2020) 15618–15625.
[34] J. Guo, Y. Ping, H. Ejima, et al., Angew. Chem. Int. Ed. 53 (2014) 5546–5551.
[35] M.A. Rahim, G. Lin, P.P. Tomanin, et al., ACS Appl. Mater. Inter. 12 (2020) 3746–3754.
[36] Y. Xu, R. Rothe, D. Voigt, et al., Nat. Commun. 12 (2021) 2407.
[37] M.A. Rahim, F. Centurion, J. Han, et al., Adv. Funct. Mater. 31 (2020) 2007336.
[38] H. Tian, B. Li, S.E. Evivie, et al., Int. J. Mol. Sci. 19 (2018).
[39] N.S. Terefe, M.A. Augustin, Crit. Rev. Food Sci. 60 (2020) 2887–2913.
[40] D. Ribeaucourt, G.T. Hofler, M. Yemloul, et al., ACS Catal. 12 (2022) 1111–1116.
[41] T.H. Kim, S.H. Kang, J.E. Han, et al., ACS Catal. 10 (2020) 4871–4878.
[42] M.M. Kaminski, O.O. Abudayyeh, J.S. Gootenberg, et al., Nat. Biomed. Eng. 5 (2021) 643–656.
[43] M. You, Z. Li, S. Feng, et al., Trends Biotechnol. 38 (2020) 637–649.
[44] H. Ravan, M. Amandadi, N. Sanadgol, Microb. Pathogenesis 91 (2016) 161–165.